RSC Advances

PAPER

View Article Online
View Journal | View Issue

Cite this: *RSC Adv.*, 2021, **11**, 390

Revealing a masked Verwey transition in nanoparticles of coexisting Fe-oxide phases

David González-Alonso, †*[a] Jesús González,[a] Helena Gavilán,[b] Jeppe Fock, ‡[c] Lunjie Zeng,[d] Kerstin Witte,§[e] Philipp Bender, ¶[a] Luis Fernández Barquín[a] and Christer Johansson[f]

Received 29th October 2020
Accepted 7th December 2020

DOI: 10.1039/d0ra09226f

rsc.li/rsc-advances

The attractive electronic and magnetic properties together with their biocompatibility make iron-oxide nanoparticles appear as functional materials. In Fe-oxide nanoparticle (IONP) ensembles, it is crucial to enhance their performance thanks to controlled size, shape, and stoichiometry ensembles. In light of this, we conduct a comprehensive investigation in an ensemble of *ca.* 28 nm cuboid-shaped IONPs in which all the analyses concur with the coexistence of magnetite/maghemite phases in their cores. Here, we are disclosing the Verwey transition by temperature dependent (4–210 K) Raman spectroscopy.

Considered as the oldest known magnetic material, magnetite (Fe_3O_4) has been revealed as a prototypical multifunctional material in the last decades.[1–7] The renewed interest is especially connected to applications associated with the reduction of such a compound to the nanoscale. Some of its fascinating applications are related to electronics and magnetism,[1–3] catalysis[4,5] and especially in biomedicine,[6,7] in which the use of magnetic ensembles of IONPs are gathering increasing attention. One of the reasons relies on their biocompatibility, which enables them to be used as vectors for drug delivery, therapeutic instruments for hyperthermia therapy, and contrast agents for magnetic resonance imaging.[7–9]

Current progress in the uniform synthesis of controllable IONPs in size and shape has unfolded their potentialities.[8,10–12] To investigate their structure and magnetic properties, a variety of techniques are required. X-ray diffraction, transmission electron microscopy (TEM), dynamic light scattering, and DC-magnetization are commonly used techniques.[13] It is widely known that magnetite IONPs may experience a progressive oxidation to maghemite (γ-Fe_2O_3) and which consequently changes their properties. However, examining the existence of magnetite within an ensemble of IONPs remains a challenging task, despite the enormous effort devoted to the study of these compounds.

The Verwey transition that characterizes magnetite could shed light on this issue.[14] Though it still remains contentious,[15] this complex phase transition involving magnetic, electric, and structural degrees of freedom[16] is extremely sensitive to oxygen vacancies.[17,18] That is the reason why it was frequently found that the characteristic Verwey transition appeared inhibited in oxidized magnetite. X-ray diffraction may help to identify magnetite,[18] whereas Mössbauer spectroscopy pinpoints magnetite by quantifying the presence of Fe^{2+} ions in the sample.[19]

Recently, this transition has been positively observed in magnetite nanocrystals (above 10 nm) by different techniques, *i.e.*, heat capacity, conductance, magnetization, nuclear magnetic resonance, and tunneling microscopy.[20–22] However, the Verwey transition can be hampered depending upon the particle size and shape.[11,20,23,24] The transition is not observed in small spherical IONPs, whereas it is clearly exhibited in cuboid-shaped nanoparticles (NPs) of similar size.[23] We associate the masked Verwey transition in spherical Fe_3O_4 NPs with surface effects that not only do increase the spin disorder along with the oxygen vacancies at the surface, but also reduce the saturation magnetization.[25] Additional studies show similar phenomena in IONPs with defects in their cores.[26] This underlines the importance of the surface anisotropy[27] to detect the Verwey transition in nanosized (4–15 nm) Fe_3O_4 NPs.

In this work, we are providing direct evidence of a masked Verwey transition in IONPs with coexisting Fe_3O_4/γ-Fe_2O_3 phases by Raman spectroscopy. The ensemble of IONPs has been carefully selected with a mixture of Fe_3O_4/γ-Fe_2O_3 and a controlled size and shape. To assess our findings, a thorough study has been conducted to characterize the IONPs.

[a]*Department CITIMAC, Faculty of Science, University of Cantabria, 39005 Santander, Spain*
[b]*Instituto de Ciencia de Materiales de Madrid, ICMM/CSIC, 28049 Madrid, Spain*
[c]*Technical University of Denmark, 2800 Kongens Lyngby, Denmark*
[d]*Chalmers University of Technology, 41296 Göteborg, Sweden*
[e]*Institute of Physics, University of Rostock, 18051 Rostock, Germany*
[f]*RISE Research Institutes of Sweden, 411 33, Göteborg, Sweden*
† Present address: Departament of Physics, Campus de Viesques, University of Oviedo, 33203 Gijón, Spain.
‡ Present address: Blusense Diagnostics Aps, DK-2100, Denmark.
§ Present address: Leibniz Institute for Plasma Science and Technology, Felix-Hausdorff-Str. 2, 17489 Greifswald, Germany.
¶ Present address: Heinz Maier-Leibnitz Zentrum (MLZ), Technische Universität München, D-85748 Garching, Germany.

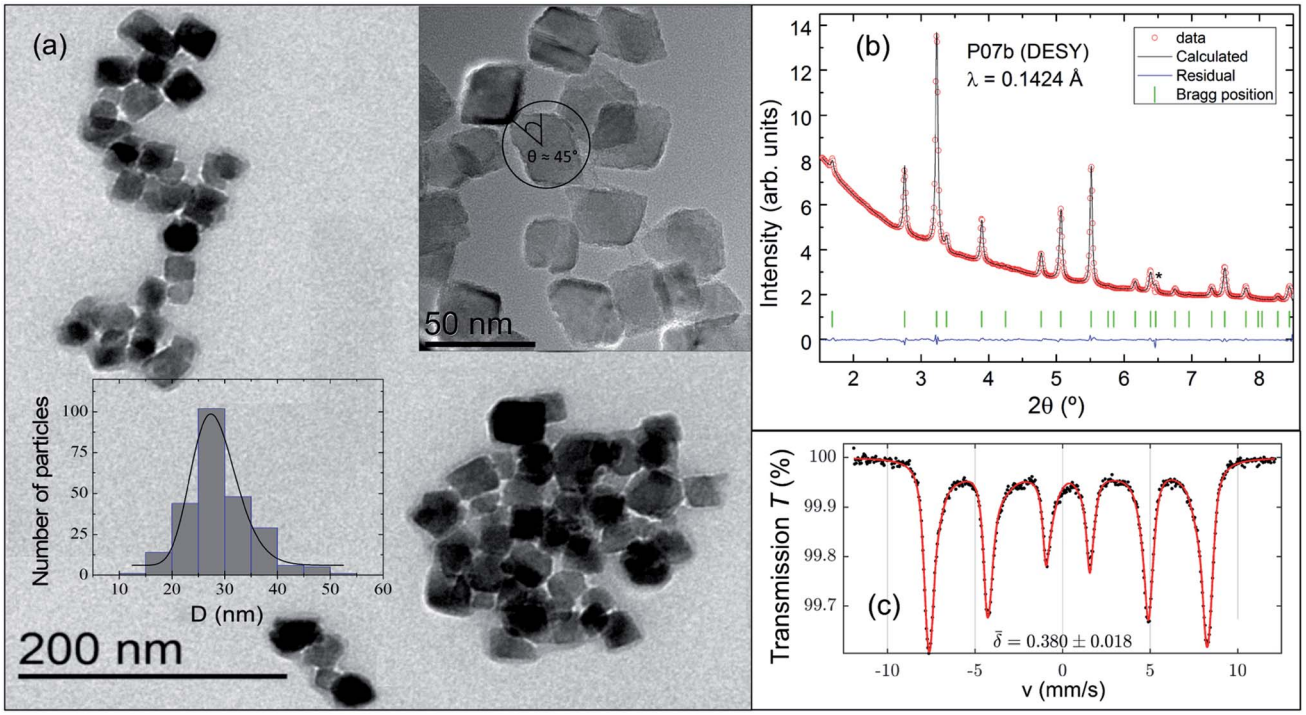

Fig. 1 (a) TEM images of single-core IONPs with cuboid shaped. At the top inset it is shown an HRTEM image of the IONPs. The black circle delimits the crystal-size used to evaluate the TEM size. The size-distribution is displayed at the bottom inset. (b) RT Rietveld refinement of the synchrotron powder diffraction pattern. * designates a small glitch during the measurement. (c) RT Mössbauer spectrum to determine the isomer-shift variation. Red line indicates the global fit, whereas black dots are the experimental data.

Additionally, other magnetite counterparts are included here to draw a complete comparison.

The IONPs were synthesized by an oxidative precipitation process described elsewhere,[28,29] followed by a dextran coating procedure under high-pressure homogenization conditions. Finally, the IONPs were magnetically fractionated using a commercial magnetophoresis setup SEPMAG-Q100 system to refine size inhomogeneities.[29] Transmission electron microscopy (TEM) and high-resolution transmission electron microscopy (HRTEM) were performed, respectively, in a FEI Tecnai G2 T20 (equipped with LaB6 electron gun) and a FEI Titan 80-300. In both cases the sample was prepared by depositing droplets of water-dispersed IONPs on a carbon-coated copper grid. The transmission high-energy X-ray diffraction (XRD) study was conducted in Debye–Scherrer geometry at HEMS beamline P07b located at PETRAIII (DESY), Hamburg (Germany). A Si (220) monochromator was used to select a wavelength of $\lambda = 0.1424$ Å.[30,31] The diffraction pattern was collected with a Perkin Elmer image plate detector, characteristic of a resolution of 2048 × 2048 pixels and a pixel size of 200 μm, at a sample to detector distance of 1254 mm. The experimental setup was calibrated using a standard Al_2O_3 powder. The transmission Mössbauer spectrum was recorded at room-temperature (RT) with a built in-house Mössbauer spectrometer equipped with a ^{57}Co source in Rh foil and operating in constant acceleration mode. Specific heat C_P was measured within the temperature range 5 K ≤ T ≤ 300 K. A standard two-τ relaxation method was used to obtain the absolute value of C_P in a Quantum Design PPMS-system. Prior to the $C_P(T)$ measurement, the IONPs powder was compressed into a pellet of 5 mm diameter and a thickness of *ca.* 1 mm. To guarantee a good thermal contact, apiezon N grease was used to stick the sample to the sample holder. Instrumental (and adhesive grease) contributions to the $C_P(T)$ signal have been subtracted. Magnetic AC-susceptibility was performed in a Quantum Design MPMS-system at a frequency of 0.5 Hz using a field amplitude of $\mu_0 H_{ac} \approx 0.3$ mT. Unpolarized micro-Raman scattering measurements were carried out with a triple monochromator Horiba-Jobin-Yvon T64000 spectrometer in subtractive mode backscattering configuration, equipped with a Horiba Symphony liquid-nitrogen-cooled CCD detector. The 647 nm line of a Coherent Innova 70Ar+-Kr+ laser was focused on the sample with a 20× objective for micro-Raman, and the laser powder was kept below 2 mW to avoid heating effects. The laser spot was 20 μm in diameter and the spectral resolution was better than 0.6 cm^{-1}. An Oxford Microstat He optical cryostat attached to the Raman microscope

Table 1 Results from the Rietveld refinement (see Fig. 1(b)) using the cubic $Fd\bar{3}m$ space group at RT [Fe_A-site at (1/8, 1/8, 1/8), Fe_B-site at (1/2, 1/2, 1/2), O at (u, u, u)]. The Goodness of fit χ^2 and standard agreement factors R_p, R_{wp}, R_{Bragg} are 3.5, 6.9%, 5.8% and 1.4%, respectively

Parameters	RT-values
Oxygen coordinate u	0.2528(1)
Lattice parameter, a (Å)	8.3741(1)
Crystal size, D (nm)	20(1)
Strain, ε ($^0/_{000}$)	24(3)

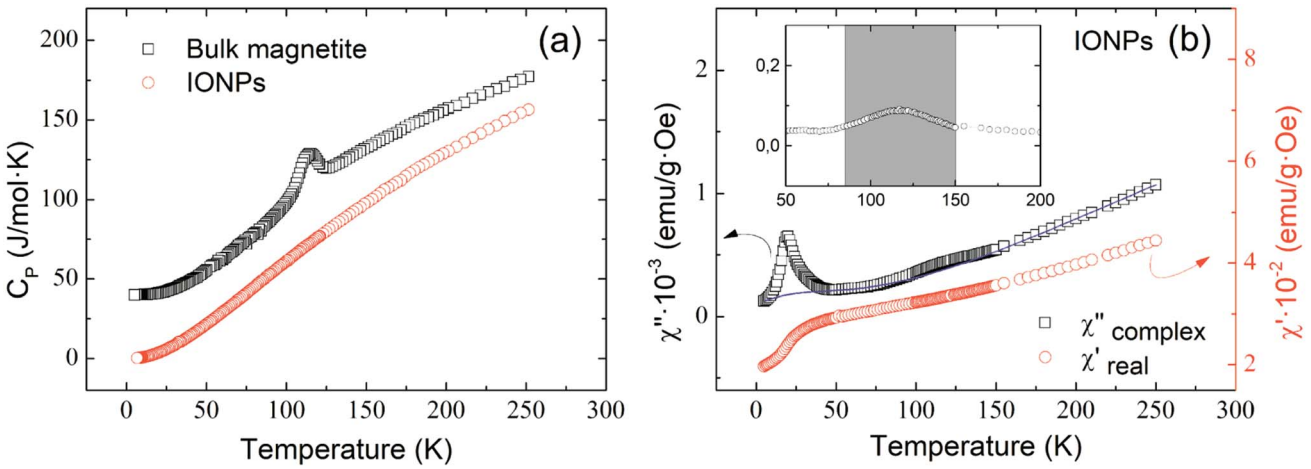

Fig. 2 (a) Specific heat of bulk magnetite and IONPs. (b) Temperature evolution of the real $\chi'(T)$ and complex $\chi''(T)$ contributions to the AC-susceptibility at the frequency of 0.5 Hz. The inset shows the position of the weak hump in $\chi''(T)$ after subtracting the solid line, for clarity.

was used for temperature-dependent measurements between 4 and 210 K.

Fig. 1(a) shows a representative TEM image of an ensemble of single-core IONPs displaying a variety of aggregates ranging from 4 units up to several dozens. The synthesis method produces cuboid-shaped IOPNs with nearly monodispersed single-cores as it is illustrated in Fig. 1(a). The size-distribution was examined with TEM by counting 250 particles (see bottom-

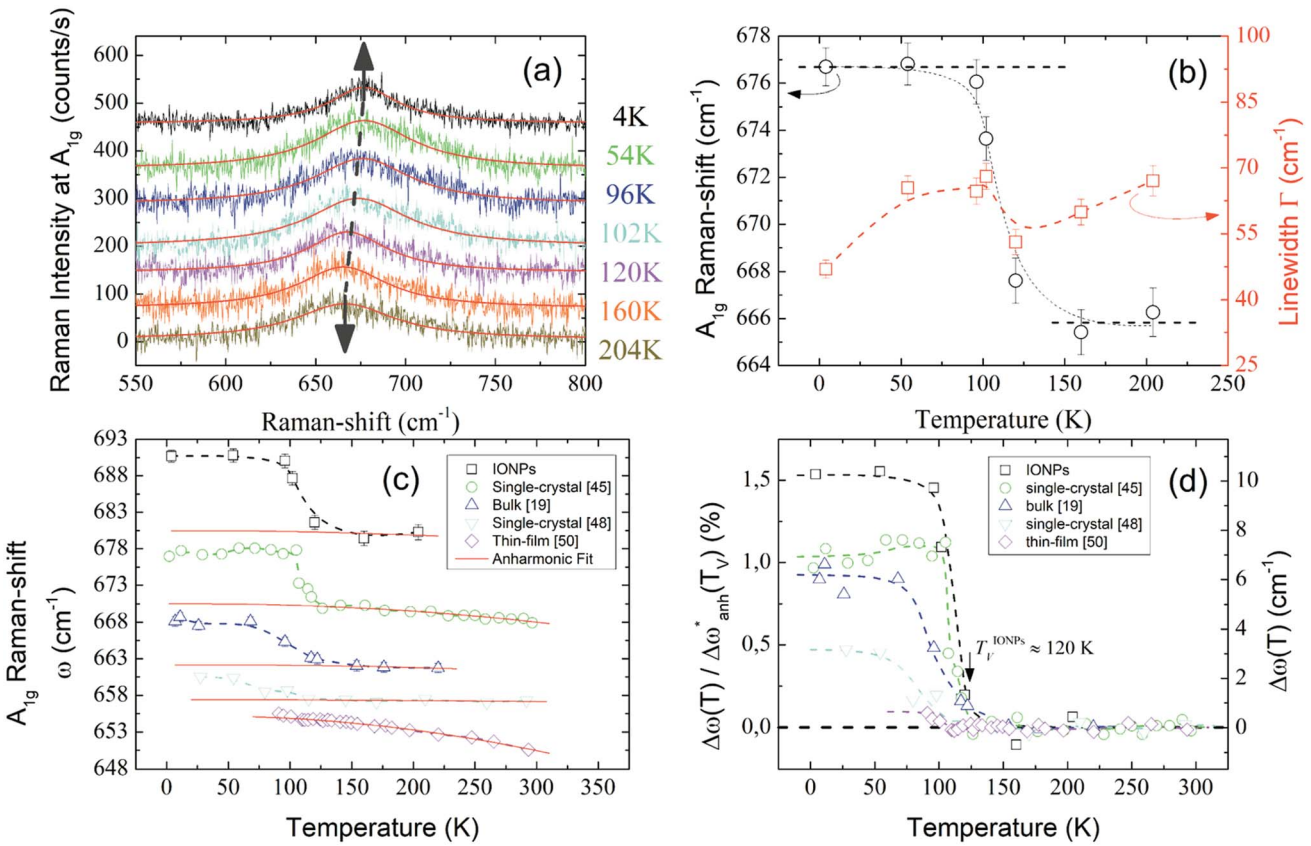

Fig. 3 (a) Raman spectra of the A_{1g} mode. Arrows indicate the shift in the frequency. Solid red lines are the Lorentzian fits. (b) Thermal evolution of both Raman-shift (black circles) and linewidth (red squares) of the A_{1g} mode around T_V. (c) A_{1g} Raman-shift of different samples are displayed for comparison and summarized in Table 2. Raman spectra have been vertically displaced for clarity. Solid red curves are the fits of the anharmonic contribution (d) Relative frequency change $\Delta\omega(T)/\Delta\omega'_{anh}(T_V)$ (left axis) and frequency change $\Delta\omega$ (right axis) of the A_{1g} mode after subtracting the harmonic term w_0 and the anharmonic contributions. Dashed lines are guides to the eye.

left inset of Fig. 1(a)). A number-weighted mean value of 28 nm with a standard deviation of 4 nm was obtained using a log-normal distribution.

In Fig. 1(b) we show the Rietveld refinement of the synchrotron XRD pattern using the FULLPROF program.[32] It should be noted that magnetite crystallizes at RT in an inverse-spinel with a cubic $Fd\bar{3}m$ space group,[33] whereas maghemite can present different crystal structures depending on the vacancy ordering.[34] Bearing this in mind, the analysis satisfactorily accounts for all the reflections with a lattice parameter of $a = 8.3741(1)$ Å. This value suggests the presence of a mixture of maghemite (γ-Fe_2O_3, $a \approx 8.34$ Å (ref. 35)) and magnetite phases (Fe_3O_4, $a \approx 8.40$ Å (ref. 36)) in the core of the IONPs. The main structural parameters refined at RT, together with the agreement factors, are compiled in Table 1. The average crystal-size obtained from the Rietveld refinement is slightly deviated from the size estimated with TEM by a factor of *ca.* 0.7. We can properly explain this mismatch by applying the correction factor proposed for cuboid-shaped NPs,[37] $D_{\text{Rietveld}} \approx \langle D_{\text{TEM}} \rangle \cdot \cos(\pi/4)$, as depicted in the top-right inset of Fig. 1(a). Therefore, the average size obtained with TEM and XRD (synchrotron) is *ca.* 28 nm.

Fig. 1(c) displays the Mössbauer spectrum conducted at RT. Provided the $\overline{\delta_{\text{RT}}}$ isomer-shift variation obtained from the analysis of the RT Mössbauer data, Fock and Bogart *et al.* showed that a quantitative evaluation of the amount of magnetite is feasible in solid-solutions of mixed maghemite-magnetite phases.[19] The evaluation of the amount of magnetite is estimated through the expressions $\alpha = \frac{(\overline{\delta_{\text{RT}}} - \delta_0)}{m}$ and $w \approx \frac{28.94\alpha}{29.94 - \alpha}$. The quantity α designates the atomic percentage of Fe^{2+} ions in the sample, whereas w indicates the weight percentage of magnetite. The parameters δ_0 and m are evaluated to be 0.321 ± 0.002 mm s^{-1} and 0.21 ± 0.01 mm s^{-1}, respectively, by the calibration-curve described in.[19] In this ensemble of IONPs, the corresponding $\overline{\delta_{\text{RT}}}$ is 0.38 ± 0.02 mm s^{-1}, and consequently a weight percentage of 28 ± 10 (wt%) in magnetite is estimated. Therefore, the structural analysis conveys that our ensemble of IONPs constitutes a good example of coexisting Fe_3O_4/γ-Fe_2O_3 phases.

Fig. 2(a) shows the temperature dependence of specific heat for the ensemble of IONPs (red circles) and for a bulk polycrystalline magnetite sample (black squares) for comparison. It is worth noting that no distinctive peak is observed for the IONPs, whereas the bulk magnetite exhibits the characteristic peak identifying the Verwey transition at *ca.* 114 K.[38,39] Fig. 2(b) depicts the temperature evolution of the real $\chi'(T)$ and the complex $\chi''(T)$ components of the AC-susceptibility.[16] No trace of the Verwey transition is observed neither in $\chi'(T)$ nor in zero-field-cooled DC-magnetization (not shown here). However, a low-temperature kink (below 50 K) is perceived in Fig. 2(b). This is usually associated with magnetic clustering (spin-glass-like transition) of IONPs,[40] but it has also been related to spin polarization effects.[41,42] Additionally, $\chi''(T)$ exhibits an absorption peak at $T \approx 27$ K that is surely connected with the mentioned magnetic clustering of IONPs. For the work presented here, it is relevant to ascertain the presence of magnetite as a very weak hump appearing centered around 120 K and illustrated in the inset of Fig. 2(b). In view of this result, we surmise that this feature provides a feeble indication of the Verwey transition in the ensemble of IONPs.[15,43]

Table 2 Parameters characterizing the A_{1g} Raman active mode for different Fe_3O_4 samples undergoing the Verwey transition, *i.e.*, frequency change $\Delta\omega$, relative frequency change $\Delta\omega/w_0$, Verwey transition temperature T_V and transition temperature span ΔT

$\Delta\omega$ (cm^{-1})	$\Delta\omega/w_0$	T_V[a] (K)	ΔT (K)	A (cm^{-1})	B (cm^{-1})	Fe_3O_4 samples
~10	~1.5	~120	~11	1.39	−0.92	IONPs
~7	~1.0	~120	~14	2.58	−1.59	Single-crystal[45]
~6	~0.9	~114	~30	1.37	−0.71	Bulk magnetite[19]
~3.4	~0.5	~121	~48	0.012	−0.11	Single-crystal[48]
~0.5	~0.1	~119	~9	1.1	−2.2	Thin-film[50]

[a] T_V appears to coincide with the temperature at which the frequency starts to vary upon cooling.

Unpolarized Raman spectra recorded at temperatures well below and above the Verwey transition temperature (T_V) are represented in Fig. 3(a). In the spectra, a clear peak around 670 cm^{-1} is visible for all temperatures between 4-210 K. This peak must be related to an active Raman mode. To understand the origin of such a peak it is necessary to briefly review the theoretical expectations governing the Raman modes. According to group theory and considering that magnetite crystallizes in a cubic inverse-spinel structure, the irreducible modes in the cubic phase at the zone center are the following:[44]

$$\Gamma = A_{1g}(R) + E_g(R) + 3T_{2g}(R) + 2A_{2u}(S) + 2E_u(S) + 5T_{1u}(IR) + 2T_{2u}(S) \quad (1)$$

where R, IR and S designate Raman, infrared and silent modes, respectively. As a result, five Raman-active modes are expected at temperatures above T_V, *i.e.*, A_{1g} at *ca.* 669 cm^{-1}, E_g at *ca.* 410 cm^{-1} and $3T^i_{2g}$ modes at *ca.* 193 (T^1_{2g}), *ca.* 540 (T^2_{2g}) and *ca.* 300 cm^{-1} (T^3_{2g}).[45,46] On the other hand, as the temperature is reduced below T_V, the symmetry of the magnetite crystal lowers to a monoclinic structure.[33,47] This complicates the low-temperature analysis because of the increasing number of Raman active modes resulting from the symmetry reduction.[48] However, Gasparov *et al.* observed that the A_{1g} mode of the parent phase persisted over the transition in the low-temperature phase.[45] They noticed a simultaneous change in both frequency and linewidth through T_V. Moreover, the broadening of the A_{1g} mode is consistent with neutron and synchrotron diffraction experiments in the vicinity of the Verwey transition.[33,47,49] The small lattice distortions (<0.24 Å) observed between the parent and the low-temperature phases must be closely connected with the softening of this phonon. In view of this, the softening of the A_{1g} mode not only does confirm the first-order phase transition undergoing at T_V,[47] but also evinces the sensitivity of this mode with respect to the Verwey transition. Therefore, following the work of Gasparov *et al.*[45] we have kept track of the thermal evolution of the A_{1g} mode across

T_V since it presents the strongest signal to monitor the Verwey transition.

In light of the above considerations, in Fig. 3(a) the arrows are indicative of the A_{1g} Raman-shift across T_V. Solid red lines represent the fitting to a Lorentzian function, $(w) = \frac{I_0 {\Gamma_0}^2}{4(w - w_0)^2 + {\Gamma_0}^2}$, where Γ_0, ω_0, and I_0 are the phonon linewidth (full width at half maximum), frequency, and intensity of the Raman scattering, respectively. The frequency and linewidth of the A_{1g} mode hallmarking the Verwey transition are clearly depicted in Fig. 3(b). The thermal evolution of the frequency shows a clear increase of *ca.* 10 cm^{-1} across T_V upon cooling. Moreover, the linewidth draws a monotonous reduction down to a temperature around 110 K from which it experiences a sudden variation nearby T_V.[50] All these phenomena confirm the transition around T_V.

In Fig. 3(c) we compare the A_{1g} Raman-shift of the ensemble of IONPs with respect to other investigated magnetite samples (bulk,[19] single-crystals,[45,48] and thin-film[50]) close to T_V. There, all samples show a jump in the Raman-shift at a similar temperature, however in the thin-film case, the frequency variation is extremely small in comparison. To account for the temperature dependence of the Raman-shift of a phonon, one can write:[50,51]

$$w(T) = w_0 + \Delta w_{\text{latt}}(T) + \Delta w_{\text{anh}}(T) = \Delta w_{\text{latt}}(T) + \Delta w^*_{\text{anh}}(T) \quad (2)$$

where w_0 is the harmonic frequency of the mode, and Δw_{latt} is ascribed to lattice distortions. The latter contribution is usually approximated by the Grüneisen law as $\left(\frac{\Delta w}{w_0}\right)_{\text{latt}} = -\gamma_{A_{1g}}\left(\frac{\Delta V}{V}\right)$. Regarding the reported Grüneisen parameter of this mode $\gamma_{A1g} = 0.96$,[52] and the small relative volume change $(\Delta V/V)_{Fe3O4}$ across T_V that varies from *ca.* 0.2% (ref. 53) to 0.004%,[54] this term does not explain alone the change in the frequency displayed in Fig. 3(c).

Below we perform the subtraction of the anharmonic contribution and the harmonic frequency to highlight the intrinsic change across T_V. For this, we evaluate the $\Delta w^*_{\text{anh}}(T)$ term. This term represents the anharmonic effects of phonon–phonon interactions at a constant volume, along with the harmonic frequency w_0, and can be described by the following equation:[55]

$$\Delta w^*_{\text{anh}} = w_0 + A\underbrace{\left(1 + \frac{2}{e^x - 1}\right)}_{\text{3-phonon}} + B\underbrace{\left(1 + \frac{3}{e^y - 1} + \frac{3}{(e^y - 1)^2}\right)}_{\text{4-phonon}} \quad (3)$$

where $x = \hbar w_0/2k_BT$ and $y = \hbar w_0/3k_BT$ correspond to three- and four-phonon interaction, respectively; and A and B are constants that are indicative of the strengths of the interaction (listed in Table 2). Except for the thin-film[50] and for the single-crystal,[48] the three-phonon interaction is predominant in all samples. For comparison, we show in Fig. 3(c) the Raman-shift of the mentioned magnetite samples. The fits to eqn (3) of the anharmonic contribution $(\Delta w^*_{\text{anh}}(T))$ are represented by solid red lines, and their main parameters are compiled in Table 2. The fit adequately describes the behavior above the transition. However, other contributions are needed to explain the variation of the frequency below T_V, *e.g.*, electron–phonon interactions.[56] The fine interpretation of these interactions is restricted to highly stoichiometric single-crystal magnetite, and is consequently beyond the scope of this work.

In Fig. 3(d) we show the frequency change of the A_{1g} mode and the relative frequency change that are respectively defined as, $\Delta w(T) \cong w(T) - \Delta w^*_{\text{anh}}(T)$, and $\Delta w(T)/\Delta w^*_{\text{anh}}(T_V)$. Although it is difficult to draw a comparison among samples of different stoichiometry and shape, our ensemble of IONPs with coexisting Fe-phases exhibits a sharp phase transition at *ca.* 120 K with a small ΔT temperature span (see Table 2). Such a small ΔT in the IONPs is similar to the magnitudes provided in.[45,50] By comparison with the magnetite samples in Table 2, the ensemble of IONPs shows the largest frequency change (*ca.* 10 cm^{-1}) and relative frequency change (1.5%). Hereby, it needs to be considered that the spectral resolution is 0.6 cm^{-1} in the Raman-shift (see Fig. 3(b)). Hence, we surmise that the magnetite nanocrystals within the ensemble of IONPs are highly stoichiometric. We suggest that the main cause for the variety of ΔT values listed in Table 2 is caused by texture effects. This fact may merit future investigations.

In conclusion, we have performed a thorough investigation and have proven that the ensemble of IONPs are constituted of coexisting Fe_3O_4/γ-Fe_2O_3 phases with an average size of *ca.* 28 nm. No sign of the Verwey transition was noticed either by specific heat or within the real component of the AC-susceptibility. However, an extremely feeble hump appears centered at around 120 K in $\chi''(T)$. A temperature-dependent analysis of Raman scattering on the A_{1g} mode has been carried out. The outcome is a conspicuous change in the frequency at around 120 K. This has allowed us to reveal the masked Verwey transition in the ensemble of IONPs. This finding highlights Raman spectroscopy as a powerful tool for the evaluation of Fe_3O_4 existence in iron-oxide compounds and towards the improvement of synthesis routes in ensembles of IONPs.

Conflicts of interest

There are no conflicts to declare.

Acknowledgements

This work was supported by EU FP7 604448 (NanoMag) and MAT2017-83631-C3-R. Dr Norbert Schell is acknowledged for the time at the HEMS beamline, and J. F. thanks MUDP (MST-141-01415).

Notes and references

1 R. Ramos, T. Kikkawa, K. Uchida, H. Adachi, I. Lucas, M. H. Aguirre, P. Algarabel, L. Morellón, S. Maekawa, E. Saitoh and M. R. Ibarra, *Appl. Phys. Lett.*, 2013, **102**, 072413.

2 S. de Jong, R. Kukreja, C. Trabant, N. Pontius, C. F. Chang, T. Kachel, M. Beye, F. Sorgenfrei, C. H. Back, B. Bräuer, W. F. Schlotter, J. J. Turner, O. Krupin, M. Doehler, D. Zhu, M. A. Hossain, A. O. Scherz, D. Fausti, F. Novelli, M. Esposito, W. S. Lee, Y. D. Chuang, D. H. Lu, R. G. Moore, M. Yi, M. Trigo, P. Kirchmann, L. Pathey, M. S. Golden, M. Buchholz, P. Metcalf, F. Parmigiani, W. Wurth, A. Föhlisch, C. Schüßler-Langeheine and H. A. Dürr, *Nat. Mater.*, 2013, **12**, 882.

3 L. Zhang, W. Hou, G. Dong, Z. Zhou, S. Zhao, Z. Hu, W. Ren, M. Chen, C.-W. Nan, J. Ma, H. Zhou, W. Chen, Z.-G. Ye, Z.-D. Jiang and M. Liu, *Mater. Horiz.*, 2018, **5**, 991.

4 A. Pratt, L. Lari, O. Hovorka, A. Shah, C. Woffinden, S. P. Tear, C. Binns and R. Kröger, *Nat. Mater.*, 2014, **13**, 26.

5 M. Muñoz, Z. M. de Pedro, J. A. Casas and J. J. Rodriguez, *Appl. Catal., B*, 2015, **176–177**, 249.

6 Q. A. Pankhurst, J. Connolly, S. K. Jones and J. Dobson, *J. Phys. D: Appl. Phys.*, 2003, **36**, R167.

7 B. Pelaz, C. Alexiou, R. A. Alvarez-Puebla, F. Alves, A. M. Andrews, S. Ashraf, L. P. Balogh, L. Ballerini, A. Bestetti, C. Brendel, S. Bosi, M. Carril, W. C. W. Chan, C. Chen, X. Chen, X. Chen, Z. Cheng, D. Cui, J. Du, C. Dullin, A. Escudero, N. Feliu, M. Gao, M. George, Y. Gogotsi, Z. Gu, N. J. Halas, N. Hampp, R. K. Hartmann, M. C. Hersam, P. Hunziker, J. Jian, X. Jiang, P. Jungebluth, P. Kadhiresan, K. Kataoka, A. Khademhosseini, J. Kopeček, N. A. Kotov, H. F. Krug, D. S. Lee, C. M. Lehr, K. W. Leong, X.-J. Liang, M. L. Lim, L. M. Liz-Marzán, X. Ma, P. Macchiarini, H. Meng, H. Möhwald, P. Mulvaney, A. E. Nel, S. Nie, P. Nordlander, T. Okano, J. Oliveira, T. H. Park, R. M. Penner, M. Prato, V. Puntes, V. M. Rotello, A. Samarakoon, R. E. Schaak, Y. Shen, S. Sjöqvist, A. G. Skirtach, M. G. Soliman, M. M. Stevens, H.-W. Sung, B. Z. Tang, R. Tietze, B. N. Udugama, J. S. VanEpps, T. Weil, P. S. Weiss, I. Willner, Y. Wu, L. Yang, Z. Yue, Q. Zhang, Q. Zhang, X.-E. Zhang, Y. Zhao, X. Zhou, A. Grünweller and W. J. Parak, *ACS Nano*, 2017, **11**, 2313.

8 A. G. Roca, R. Costo, A. F. Rebolledo, S. Veintemillas-Verdaguer, P. Tartaj, T. González-Carreño, M. P. Morales and C. J. Serna, *J. Phys. D: Appl. Phys.*, 2009, **42**, 224002.

9 P. Tartaj, M. P. Morales, T. Gonzalez-Carreño, S. Veintemillas-Verdaguer and C. J. Serna, *Adv. Mater.*, 2011, **23**, 5243.

10 S. Sun and H. Zeng, *J. Am. Chem. Soc.*, 2002, **124**, 8204.

11 J. Santoyo Salazar, L. Perez, O. de Abril, L. T. Phuoc, D. Ihiawakrim, M. Vazquez, J. M. Greneche, S. Begin-Colin and G. Pourroy, *Chem. Mater.*, 2011, **23**, 1379.

12 R. Costo, V. Bello, C. Robic, M. Port, J. Marco, M. Morales and S. Veintemillas-Verdaguer, *Langmuir*, 2012, **28**, 178.

13 P. Bender, L. K. Bogart, O. Posth, W. Szczerba, S. E. Rogers, A. Castro, L. Nilsson, L. J. Zeng, A. Sugunan, J. Sommertune, A. Fornara, D. González-Alonso, L. Fernández Barquín and C. Johansson, *Sci. Rep.*, 2017, **7**, 45990.

14 E. J. Verwey, *Nature*, 1939, **144**, 327.

15 G. Perversi, E. Pachoud, J. Cumby, J. M. Hudspeth, J. P. Wright, S. A. J. Kimber and J. P. Attfield, *Nat. Commun.*, 2019, **10**, 2857.

16 F. Walz, *J. Phys.: Condens. Matter*, 2002, **14**, R285.

17 J. M. Honig, *J. Alloys Compd.*, 1995, **229**, 24.

18 J. B. Yang, X. D. Zhou, W. Yelon, W. J. James, Q. Cai, K. Gopalakrishnan, S. K. Malik, X. C. Sun and D. E. Nikles, *J. Appl. Phys.*, 2004, **95**, 7540.

19 J. Fock, L. K. Bogart, D. González-Alonso, J. I. Espeso, M. F. Hansen, M. Varón, C. Frandsen and Q. A. Pankhurst, *J. Phys. D: Appl. Phys.*, 2017, **50**, 265005.

20 J. Lee, S. G. Kwon, J. G. Park and T. Hyeon, *Nano Lett.*, 2015, **15**, 4337.

21 S. Lim, B. Choi, S. Y. Lee, S. Lee, H. H. Nahm, Y. H. Kim, T. Kim, J. G. Park, J. Lee, J. Hong, S. G. Kwon and T. Hyeon, *Nano Lett.*, 2018, **18**, 1745.

22 A. Hevroni, M. Bapna, S. Piotrowski, S. A. Majetich and G. Markovich, *J. Phys. Chem. Lett.*, 2016, **7**, 1661.

23 A. Mitra, J. Mohapatra, S. S. Meena, C. V. Tomy and M. Aslam, *J. Phys. Chem. C*, 2014, **118**, 19356.

24 H. Gavilán, O. Posth, L. K. Bogart, U. Steinhoff, L. Gutiérrez and M. Puerto Morales, *Acta Mater.*, 2017, **125**, 416.

25 Z. Nedelkoski, D. Kepaptsoglou, L. Lari, T. Wen, R. A. Booth, S. D. Oberdick, P. L. Galindo, Q. M. Ramasse, R. F. L. Evans, S. Majetich and V. K. Lazarov, *Sci. Rep.*, 2017, **7**, 45997.

26 E. Wetterskog, C. W. Tai, J. Grins, L. Bergström and G. Salazar-Alvarez, *ACS Nano*, 2013, **7**, 7132.

27 G. Salazar-Alvarez, J. Qin, V. Sepelák, I. Bergmann, M. Vasilakaki, K. N. Trohidou, J. D. Ardisson, W. Macedo, M. Mikhaylova, M. Muhammed, M. Baró and J. Nogués, *J. Am. Chem. Soc.*, 2008, **130**, 13234.

28 M. Andrés Vergés, R. Costo, A. Roca, J. Marco, G. Goya, C. Serna and M. P. Morales, *J. Phys. D: Appl. Phys.*, 2008, **41**, 134003.

29 C. Grüttner, K. Müller, J. Teller, F. Westphal, A. Foreman and R. Ivkov, *J. Magn. Magn. Mater.*, 2007, **311**, 181.

30 N. Schell, A. King, F. Beckmann, H. Ruhnau, R. Kirchhof, R. Kiehn, M. Müller and A. Schreyer, *AIP Conf. Proc.*, 2010, **1234**, 391.

31 N. Schell, A. King, F. Beckmann, T. Fischer, M. Müller and A. Schreyer, *Mater. Sci. Forum*, 2014, **772**, 57.

32 J. Rodríguez-Carvajal, *Phys. B*, 1993, **192**, 55.

33 M. Iizumi, T. F. Koetzle, G. Shirane, S. Chikazumi, M. Matsui and S. Todo, *Acta Cryst. B*, 1982, **38**, 2121.

34 C. Pecharromán, T. González-Carreño and J. E. Iglesias, *Phys. Chem. Miner.*, 1995, **22**, 21.

35 A. N. Shmakov, G. N. Kryukova, S. V. Tsybulya, A. L. Chuvilin and L. P. Solovyeva, *J. Appl. Crystallogr.*, 1995, **28**, 141.

36 H. Okudera, K. Kihara and T. Matsumoto, *Acta Crystallogr., Sect. B: Struct. Sci.*, 1996, **52**, 450.

37 F. Vereda, J. de Vicente, M. del Puerto Morales, F. Rull and R. Hidalgo-Álvarez, *J. Phys. Chem. C*, 2008, **112**, 5843.

38 E. F. Westrum and F. Gronvold, *J. Chem. Thermodyn.*, 1969, **1**, 543.

39 J. P. Shepherd, J. W. Koenitzer, R. Aragón, J. Spalek and J. M. Honig, *Phys. Rev. B: Condens. Matter Mater. Phys.*, 1991, **43**, 8461.

40 Z. Svindrych, Z. Janu, A. Kozlowski and J. M. Honig, *Phys. Rev. B: Condens. Matter Mater. Phys.*, 2012, **86**, 214406.
41 M. Alexe, M. Ziese, D. Hesse, P. Esquinazi, K. Yamauchi, T. Fukushima, S. Picozzi and U. Gösele, *Adv. Mater.*, 2009, **21**, 4452.
42 S. F. Alvarado, W. Eib, F. Meier, D. T. Pierce, K. Sattler, H. C. Siegmann and J. P. Remeika, *Phys. Rev. Lett.*, 1975, **34**, 319.
43 L. V. Gasparov, A. Rush, G. Güntherodt and H. Berger, *Phys. Rev. B: Condens. Matter Mater. Phys.*, 2009, **79**, 144303.
44 W. B. White and B. DeAngelis, *Spectrochim. Acta, Part A*, 1967, **23**, 985.
45 L. V. Gasparov, D. B. Tanner, D. B. Romero, H. Berger, G. Margaritondo and L. Forró, *Phys. Rev. B: Condens. Matter Mater. Phys.*, 2000, **62**, 7939.
46 J. L. Verble, *Phys. Rev. B: Solid State*, 1974, **9**, 5236.
47 M. S. Senn, J. P. Wright and J. P. Attfield, *Nature*, 2012, **481**, 173.
48 R. Gupta, A. K. Sood, P. Metcalf and J. M. Honig, *Phys. Rev. B: Condens. Matter Mater. Phys.*, 2002, **65**, 104430.
49 M. S. Senn, J. P. Wright, J. Cumby and J. P. Attfield, *Phys. Rev. B: Condens. Matter Mater. Phys.*, 2015, **92**, 024104.
50 A. Kumar, S. Chaudhary, D. K. Pandya and S. K. Sharma, *Phys. Rev. B: Condens. Matter Mater. Phys.*, 2014, **90**, 024302.
51 M. Maczka, M. Ptak, K. Hermanowicz and A. Majchrowski, *Phys. Rev. B: Condens. Matter Mater. Phys.*, 2011, **83**, 174439.
52 O. N. Shebanova and P. Lazor, *J. Chem. Phys.*, 2003, **119**, 6100.
53 J. Wright, J. Attfield and P. Radaelli, *Phys. Rev. B: Condens. Matter Mater. Phys.*, 2002, **66**, 214422.
54 J. Blasco, J. García and G. Subías, *Phys. Rev. B: Condens. Matter Mater. Phys.*, 2011, **83**, 104105.
55 M. Balkanski, R. F. Wallis and E. Haro, *Phys. Rev. B: Condens. Matter Mater. Phys.*, 1983, **28**, 1928.
56 E. Granado, A. García, J. A. Sanjurjo, C. Rettori, I. Torriani, F. Prado, R. D. Sánchez, A. Caneiro and S. B. Oseroff, *Phys. Rev. B: Condens. Matter Mater. Phys.*, 1999, **60**, 11879.